Electronic Supplementary Material (ESI) for Journal of Materials Chemistry C.

Supporting Information

Activation of carbon tow electrodes for use in iron aqueous redox systems for electrochemical applications.

Philipp Schroeder[1,2,5], Noemí Aguiló-Aguayo[2], Andrea Auer[3], Christoph Griesser[3], Julia Kunze-Liebhäuser[3], Yibo Ma[4], Michael Hummel[4], Dagmar Obendorf[1], Thomas Bechtold[2*]

[1]Institute of Analytical Chemistry and Radiochemistry

Leopold-Franzens-University Innsbruck

Innrain 80-82, A-6020 Innsbruck

[2]Research Institute of Textile Chemistry and Textile Physics**

Leopold-Franzens-University of Innsbruck

Hoechsterstraße 73 A-6850 Dornbirn, Austria

[3]Department of Physical Chemistry

Leopold-Franzens-University Innsbruck

Josef-Möller-Haus

Innrain 52c, A-6020 Innsbruck

[4]Department of Bioproducts and Biosystems

Aalto University

Vuorimiehentie 1, FI-02150 Espoo

[5]Austrian Drug Screening Institute – ADSI

University of Innsbruck

Innrain 66a

A-6020 Innsbruck

ESI-1: Effect of desizing on roving handling performance

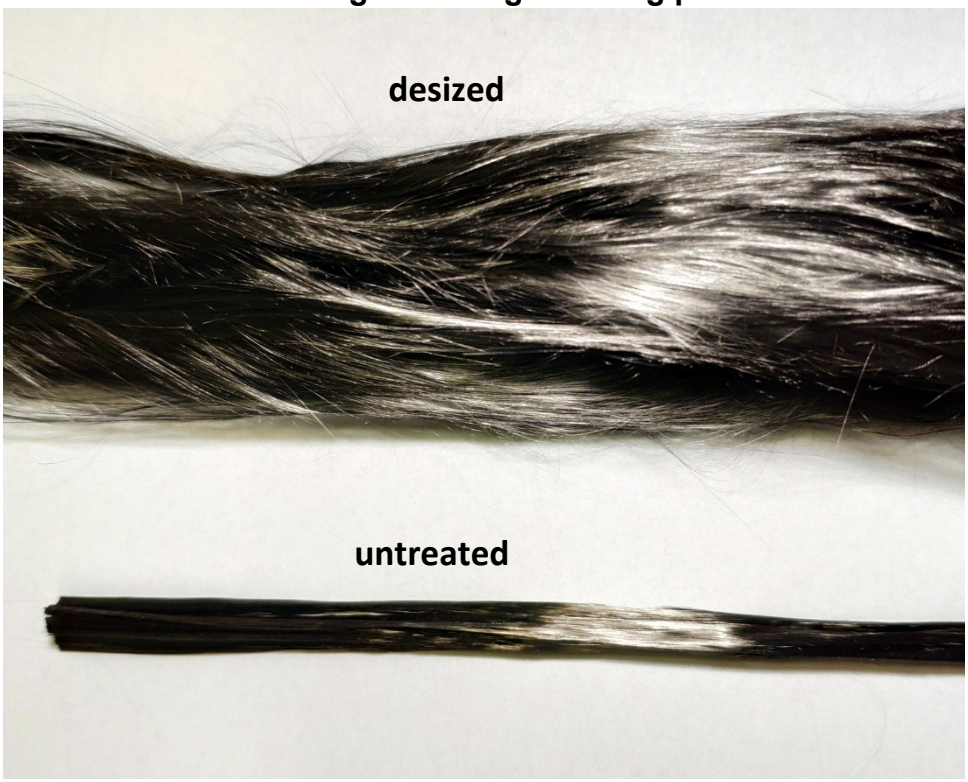

Fig. ESI-1. Desized (top) vs untreated 48k roving (bottom).

Fig. ESI-1 shows the effect of desizing on a carbon roving. The desized roving strongly disperses and the handling performance is poor.

ESI-2: FT-IR spectroscopy

The FTIR spectra were recorded as liquid film between silicon waver discs using a FTIR-spectrometer (Bruker Vector 22 FTIR Spectrometer; spectral range 4000 to 400 cm^{-1}).

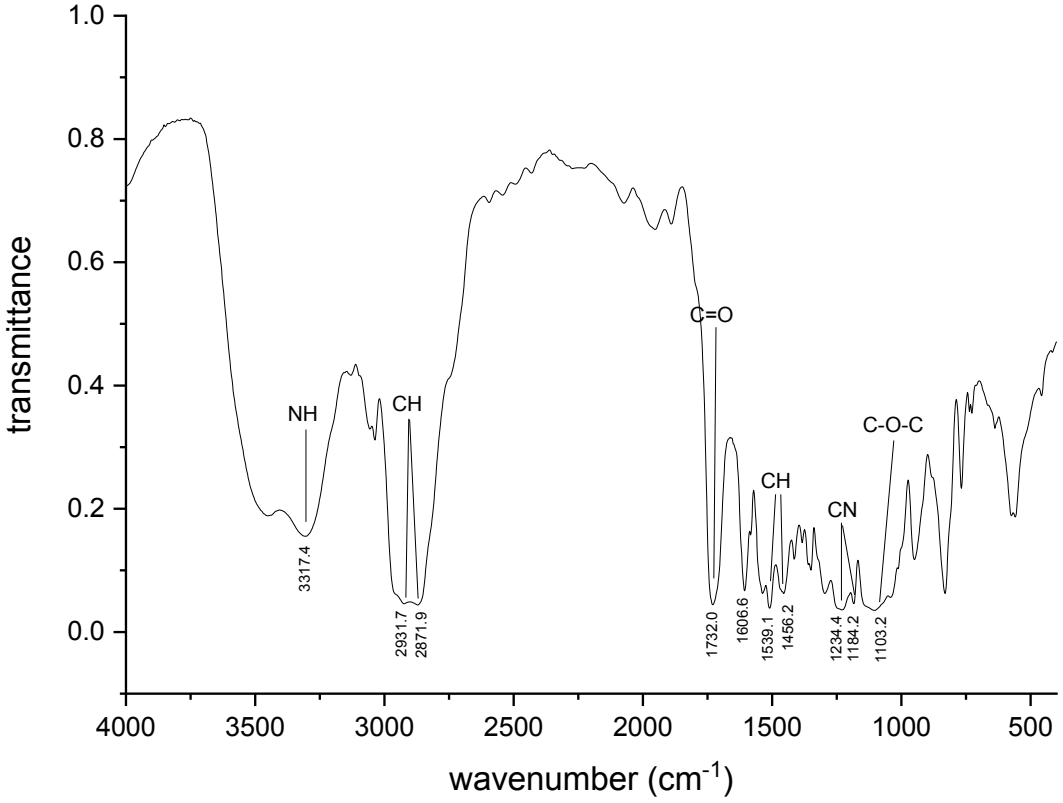

Fig. ESI-2. FT-IR of acetone extract of Toho Tenax STS 40 CF.

The extracted polymer exhibits the structural elements of a polyurethane-polyester copolymer.

In the FT-IR spectra vibrations at 3300 – 3600 cm^{-1} indicate the presence of NH and OH groups, C-H bonds are indicated with absorptions at 2931 cm^{-1} and 2871 cm^{-1}. The presence of C=O double bonds e.g. of an ester or urethane group is detected at 1732 cm^{-1} and the amide I and amide II vibrations are detected at 1606 cm^{-1} and 1539 cm^{-1} respectively. Strong absorbances due to presence of C-O and C-N bonds are observed in the fingerprint region between 1000 cm^{-1} and 1200 cm^{-1}.

ESI-3: TGA

For thermal gravimetric analysis the samples were heated in alumina cups, under nitrogen atmosphere with a heating rate of 10 K/min from 50 °C to 800 °C using a TGA unit (Mettler Toledo TGA2).

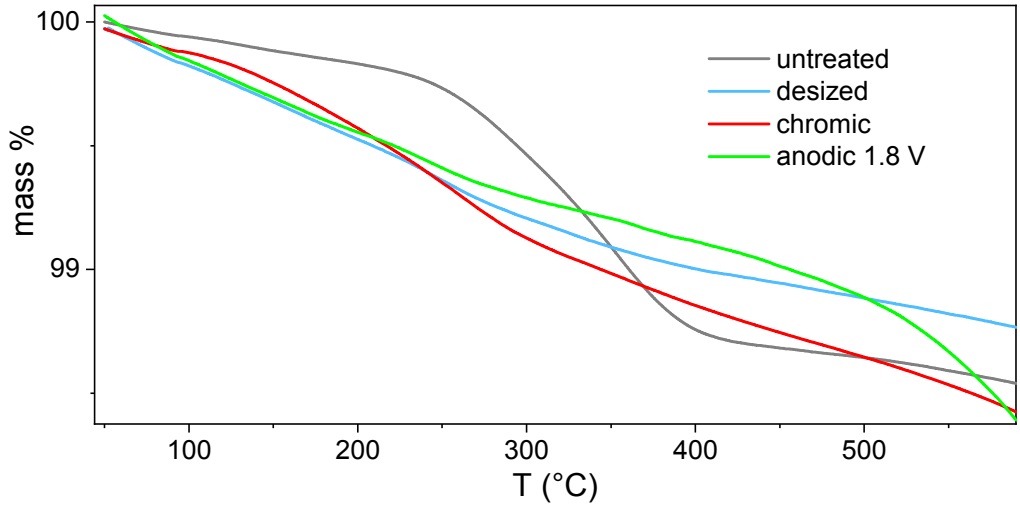

Fig. ESI-3. TGA of untreated, desized and activated CF.

Fig. ESI-3 shows the thermogravimetric analysis of untreated, desized and oxidatively pre-treated carbon rovings. The untreated roving shows a distinct 1% weight loss between 250 and 400°C. This weight loss matches the sizing amount specified by the manufacturer (1 %). This distinct step is not visible for the desized and activated fibres and indicates good removal of the sizing layer in the desizing process.

ESI-4: Electrolysis Setup

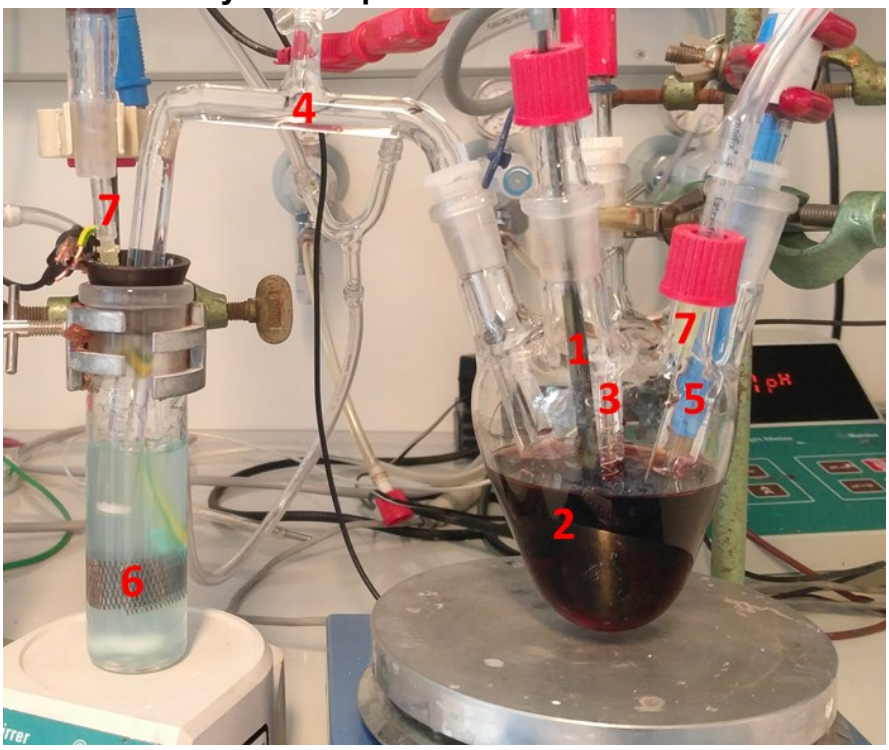

Fig. ESI-4. (1) CRLE, (2) modified phototrode, (3) Ag/AgCl reference electrode, (4) u-tube filled with background electrolyte, (5) redox electrode (Pt // Ag/AgCl 3 M KCl), (6) platinum counter electrode, (7) Ar inlet.

ESI-5: Effect of stirring speed

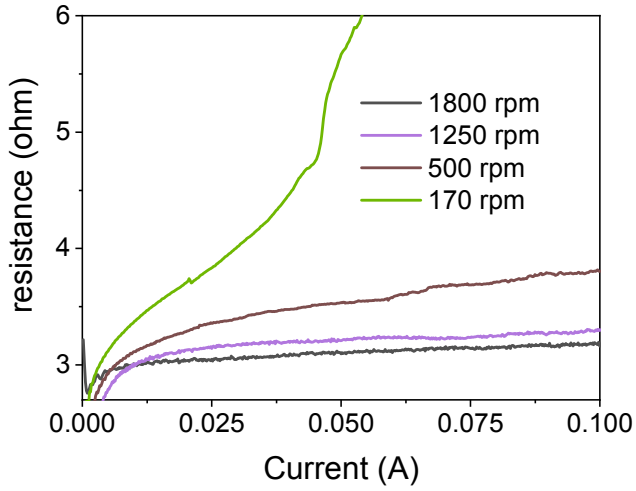

Fig. ESI-5. Galvanodynamic scan, 10 mM $[Fe(CN)_6]$ 50% SoC in 1 M Na_2SO_4, 1 mM borate, pH 9, anodically activated CLRE, effect of stirring speed on resistance (*R*) calculated in Equation 3.

Fig. ESI-5 shows a linear galvanodynamic scan from 0 to 100 mA in the constant state of charge setup (ESI-4). The resistance *R* is calculated from Equation 3. While *R* increases drastically at low stirring speeds with increasing current, a change from 1250 rpm to 1800 rpm did not significantly decrease the resistance. This indicates that the mass transport is limited by diffusion while mass transport by convection does not contribute to the electrode potential if the stirring speed is sufficiently high.

$$R = \frac{(E_{we} - E_{sol})}{I} \qquad (3)$$

ESI-6: Square wave voltammetry at differently treated CFMCEs

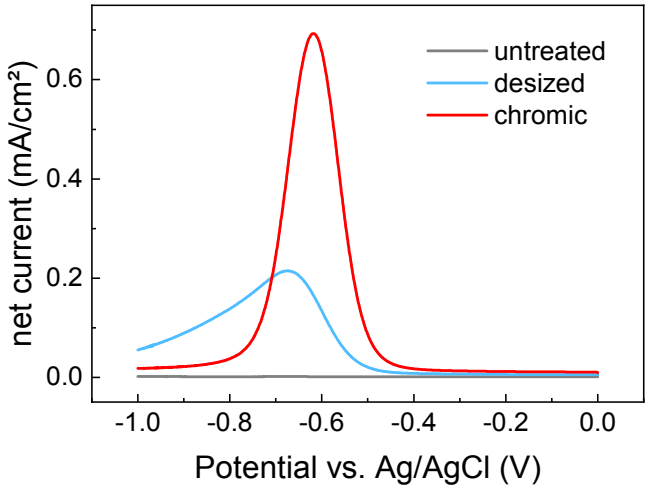

Fig. ESI-6. SWV response of untreated, desized and chromic acid dipped CFMCEs (E_{sw} = 50 mV, ΔE_s = 1 mV, f = 10 Hz), 1 mM Na[Fe^{III}-racEDDHA], background electrolyte: 1 M Na_2SO_4, 5 mM borate, pH 9.

Fig SI-5 shows the net current vs potential of three differently treated CFMCEs. While the untreated filament is electro-inactive the desized fibre shows a large peak half with and a peak potential shifted to more negative values thus, indicating sluggish electron transfer. In contrast, the chromic acid treated filament shows a narrow, symmetrical peak as expected for a reversible electron transfer.

ESI-7: Optimization of the anodic polarisation procedure

In order to improve the electrochemical activation conditions with regard to time and anodic potential the overpotential for electrolysis of [$Fe^{II/III}(CN)_6$] was evaluated as the difference between working electrode potential E_{we} and the solution potential E_{sol} from galvanostatic electrolysis experiments at constant state of charge (Eq. 1). The averaged overpotential $\bar{\eta}$ was calculated from charge/discharge overpotentials and corrected for the potential drop caused by the roving resistance R_{rov} at charge/discharge current I (Eq 2).

$$\eta = E_{we} - E_{Esol} \tag{1}$$

$$\bar{\eta} = \frac{|\eta_{charge}| + |\eta_{discharge}|}{2} - R_{rov} \times |I| \tag{2}$$

For experiments with constant state of charge (SoC), two CRLEs (working electrode and counter electrode) were placed in the same electrolyte. The electrolyte (1 M Na_2SO_4, 5 mM borate, pH 9) contained 100 mM $K_3[Fe^{III}(CN)_6]$ and 100 mM $K_4[Fe^{II}(CN)_6]$. Galvanostatic electrolysis was performed at +/-126 mA applied for 30 seconds. The electrode potential of the working electrode was collected at the end of electrolysis sequence.

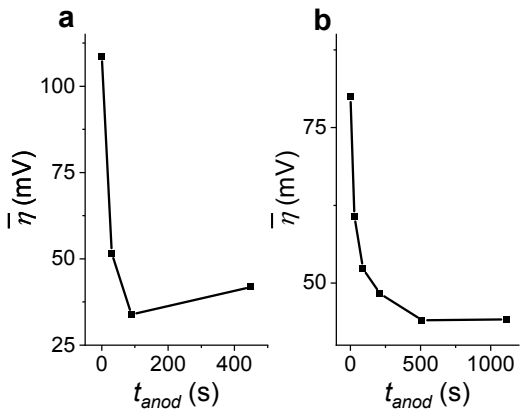

Fig. ESI-7 a) Averaged overpotential $\overline{\eta}$ of CRLEs as function of anodic polarisation: Anode potential vs. (Ag/AgCl KCl 3 M) reference: a) 1800 mV; b) 1200 mV. Electrolyte for galvanostatic electrolysis 100 mM $K_3[Fe^{III}(CN)_6]$, 100 mM $K_4[Fe^{II}(CN)_6]$, 1 M Na_2SO_4, 1 mM borate, pH 9; charge/discharge current +/- 126 mA for 30 s.

Fig. ESI-7a shows the effect of anodic activation on the averaged overpotential $\overline{\eta}$ of CRLEs for anodic activation at 1800 mV and 1200 mV electrode potential. At 1800 mV the minimum is reached after 90 seconds of current flow. During the anodic treatment a dissolution processes at the carbon surface and formation of graphene particles was indicated by a brown coloured electrolyte.[1] With longer activation time the overpotential increases again, most likely due to destruction of single filaments and therefore loss of electrode surface. A single fibre of a CFMCE broke after 360 s polarisation in 0.1 M NaOH at 1800 mV, due to the high lateral current density (Fig. ESI-7c). At an anode potential of 1200 mV the overpotential of the CRLE decreases slower and stabilises after an electrolysis time of approximately 500 s at comparable level to the activation at 1800 mV. Therefore, anodic oxidation at 1800 mV for 90 seconds was used as standard method for activation of desized CRLE.

Electrochemical preparation of free-standing few-layer graphene through oxidation–reduction cycling

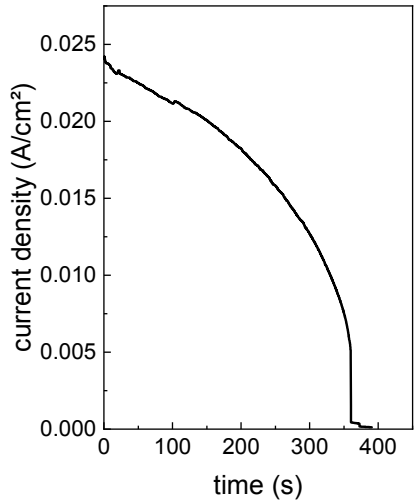

Fig. ESI-7c. Anodic polarisation current of a CFMCE at 1800 mV

ESI-8: EIS

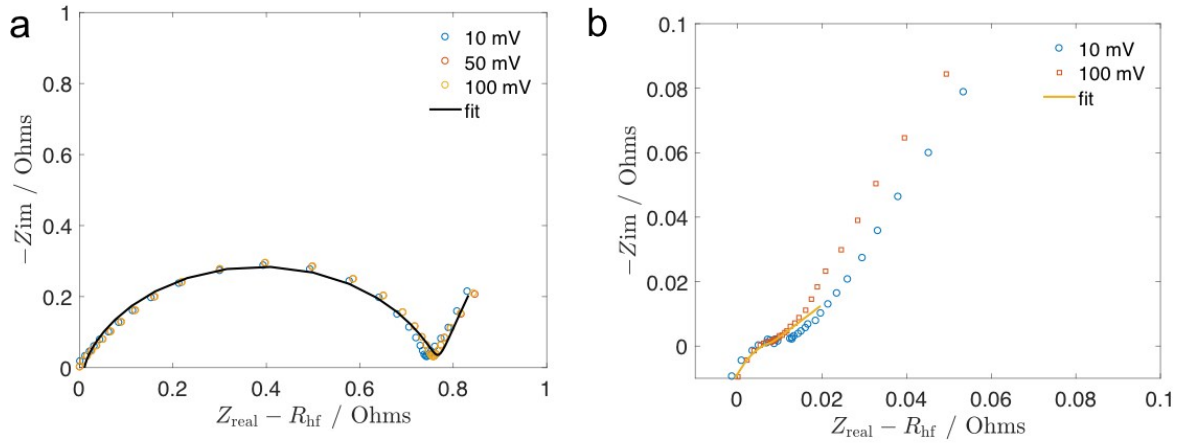

Fig. ESI-8. Typical impedance experiment; 65 mM FeCN6, 50% SoC, effect of AC amplitude, (a) desized CRLE 10/50/100 mV amplitude, (b) CRLE anodically pre-treated, 10/100 mV amplitude.

Initial EIS experiments showed well defined semi circles for desized electrodes with relatively large R_{ct} at small amplitudes, i.e. 10 mV. However, activated rovings with extremely small R_{ct} compared to R_{hf} featured noisy and poorly defined semi circles (Fig. ESI-8b) where accurate fitting was impossible. Increasing the amplitude from 10 to 100 mV improved the signal (Fig. ESI-8b) while the fit was unchanged for desized electrodes (Fig. ESI-8a).

Table ESI-8: Fitting data of impedance spectra

complex	E#	treatment	*L* (µH)	R_{hf} (Ω)	Q_{dl} (Fs^{a-1})	a	R_{ct} (Ω)	W (Ω $s^{-1/2}$)
Fe-racEDDHA	ME#48	acetone	0.193	3.021	4.3e-3	0.883	0.287	0.079
	ME#49	acetone	0	2.016	3.9e-3	0.913	0.178	0.079
	ME#48	chromic	0.522	2.250	0.017	0.671	0.081	0.056
	ME#49	chromic	0.429	2.043	0.041	0.576	0.127	0.045
	ME#50	anodic	0.476	1.734	0.020	0.648	0.094	0.055
	ME#51	anodic	0.374	2.221	0.027	0.605	0.138	0.049
$Fe(CN)_6$	ME#33	untreated	0.538	1.844	8.2e-3	0.896	13.95	0.120
	ME#53	acetone	0.118	2.416	2.9e-3	0.856	0.316	0.064
	ME#55	acetone	0	3.507	5.7e-3	0.805	0.365	0.073
	ME#52	chromic	0.464	2.863	0.020	0.627	0.067	0.084
	ME#53	chromic	0.423	2.396	0.071	0.415	0.096	0.073
	ME#54	anodic	0.496	2.279	4.8e-3	0.790	0.039	0.043
	ME#55	anodic	0.425	2.113	3.9e.3	0.895	0.017	0.033

Table ESI-8 shows the fitting data of the Randles circuit for all tested electrodes. Averages of R_{ct} and their standard deviation of the respective group are calculated and depicted in Fig. 7 (main file).

ESI-9: Additional SEM images

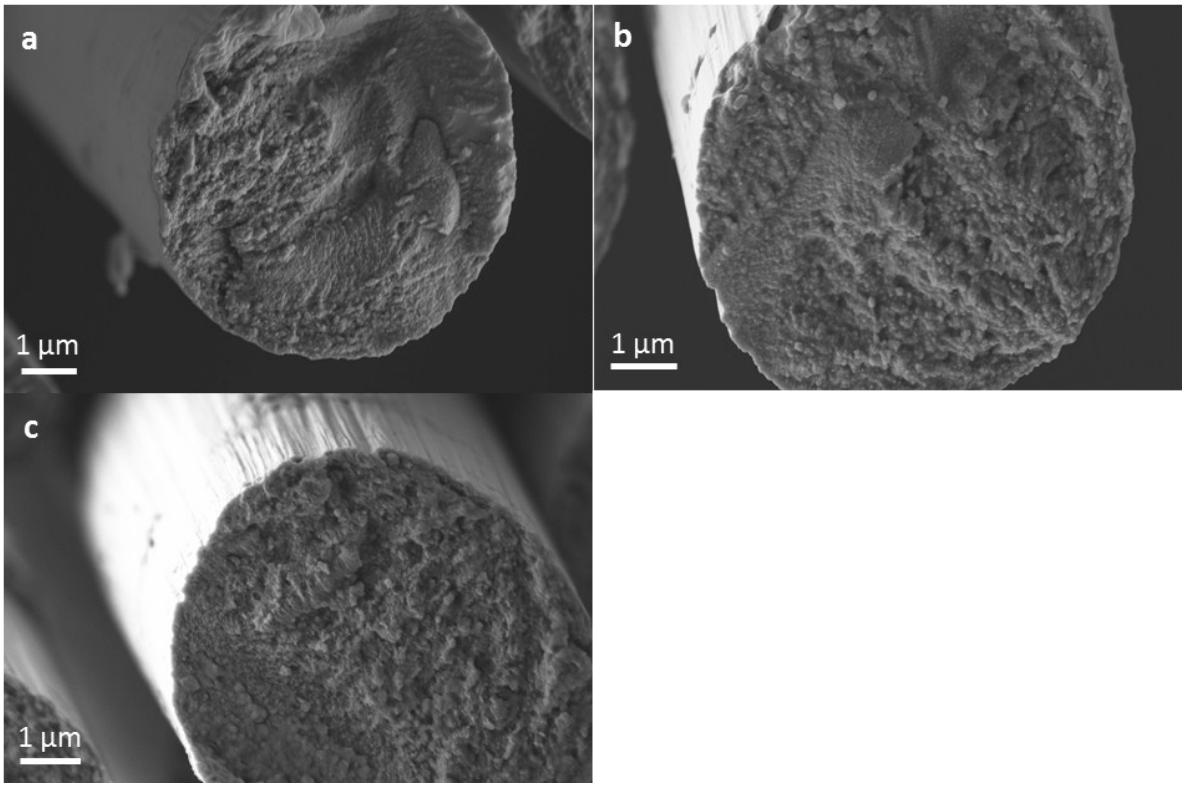

Fig. ESI-9. Cross sections of the fractured fibres. Untreated (a), desized (b) and anodically activated (c) fibre.

ESI-10: XPS spectra

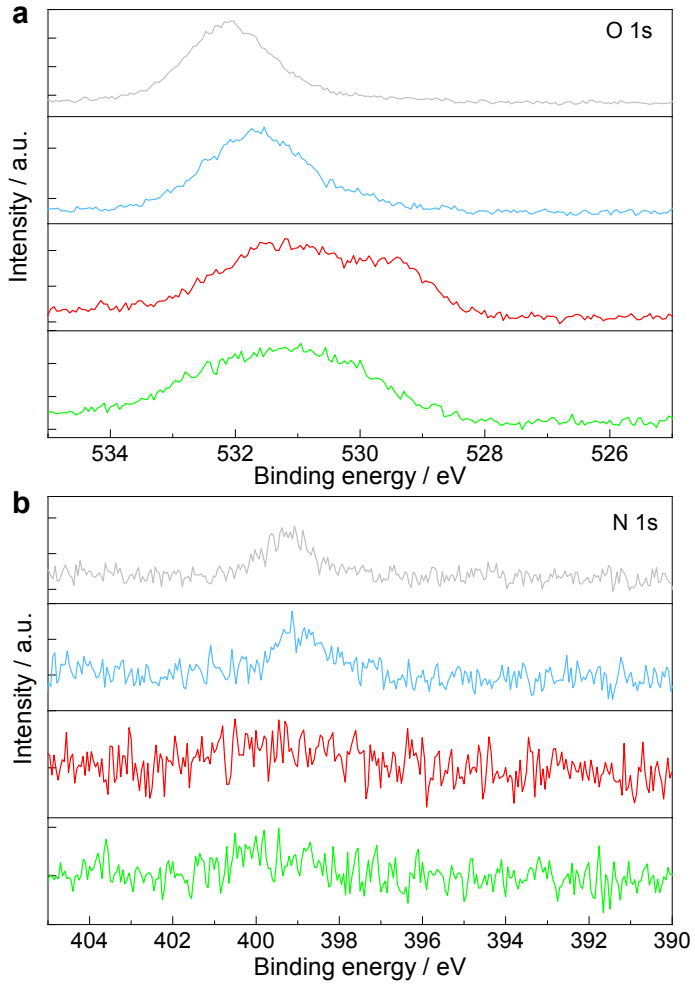

Fig. ESI-10. XPS spectra of the N 1s (a) and O 1s (b) region of the carbon rovings. The grey line is related to the untreated, the blue line the desized the red line the chromic acid treated and the green line the anodized fiber.

Table ESI-10: Peak fitting parameter.[2]

Sample	Binding energy (eV) [FWHM (eV)]				
	sp^2	**sp^3**	**C-N/C-O-C**	**C-OH**	**C=O**
Untreated	283.6 [1.3]	0*	285.4 [1.3]	0*	288.1 [1.3]
Desized	283.6 [1.3]	0*	285.4 [1.5]	0*	288.1 [1.5]
Chromic acid treated	283.7 [1.4]	285.0 [1.4]	0*	286.5 [1.4]	288.1 [1.4]
Anodized	283.7 [1.2]	284.9 [2.0]**	0*	286.4 [2.0]**	288.0 [2.0]**

* Due to the small binding energy difference between C-N/C-O-C, C-C and C-OH the small contributions of C-C and C-OH species to the C-N/C-O-C signal cannot be excluded.

** The higher FWHM values are related to effects of the inhomogeneity of the sample and the absence of distinct peaks towards the higher energy side of the C 1s spectrum.

References

1 B. Qi, L. He, X. Bo, H. Yang and L. Guo, *Chem. Eng. J.*, 2011.

2 W. M. Lau, L. J. Huang, I. Bello, Y. M. Yiu and S. T. Lee, *J. Appl. Phys.*, 1994, **75**, 3385–3391.